Griffiths-McCoy singularities in the dilute transverse-field Ising model: A numerical linked cluster expansion study

Foster Thompson
Department of Physics, Case Western Reserve University, Ohio 44106, USA

Rajiv R. P. Singh
Department of Physics, University of California Davis, California 95616, USA

(Received 21 November 2018; published 25 March 2019)

We use numerical linked cluster expansions (NLCEs) to study the site-diluted transverse-field Ising model on the square lattice at $T = 0$. NLCE with a self-consistent mean field on the boundary of the clusters is used to obtain the ground-state magnetization, susceptibility, and structure factor as a function of transverse field h and exchange constant J. Adding site dilution to the model turns NLCE into a series expansion in the dilution parameter p. Studying the divergence of the structure factor allows us to establish the phase diagram in the h/J and p plane. By studying the magnetization of the system in a longitudinal field, we investigate the Griffiths-McCoy singularities. We find that the magnetization develops nonlinearities in the Griffiths phase with exponents that vary continuously with h. Additionally, the probability distribution of the local susceptibility develops long tails in the Griffiths phase, which is studied in terms of its moments.

DOI: 10.1103/PhysRevE.99.032129

I. INTRODUCTION

Disorder occurs in physical systems for a plethora of reasons. We considered the case of site dilution—the random omission of lattice sites—in the transverse field Ising model in two dimensions. This models magnetic substances with a fixed concentration of nonmagnetic impurities and alloys of magnetic and nonmagnetic substances. Among other properties, this model displays two noteworthy features: a discontinuity in the critical value of the transverse field as a function of the dilution parameter and Griffiths–McCoy singularities.

The discontinuity in the transverse field as the dilution parameter varies below the percolation threshold was first shown by Harris [1]. Below the percolation threshold the lattice is composed of disconnected pieces, so no overall long-range order is possible. Once the lattice percolates, a cluster of spins spanning the entire length of the lattice arises, permitting long-range order up to a critical field of at least that of the one-dimensional pure system. This picture was later confirmed by Stinchcombe using a real-space renormalization-group calculation [2].

Griffiths singularities arise due to the low but nonzero probability of large nondilute regions in an otherwise dilute lattice. These regions tend to magnetize, locally entering a ferromagnetic phase despite the disordered behavior of the bulk lattice, effectively behaving as embedded, finite-size copies of the pure system [3]. These clusters lead to "Griffiths" singularities everywhere where the pure system is ordered. In classical systems, these singularities are weak as the probability of having a large ordered region falls off exponentially with size and consequently they are barely visible experimentally or numerically. However, in dynamical properties of quantum systems, tunneling between the ground state and excited states in the locally nondilute regions gives the weight of singularities an additional factor related to the inverse of energy gap between these states, which is also exponentially small in the region size. This can promote what were weak essential singularities in thermodynamic quantities into power laws. As a consequence, these quantum Griffiths-McCoy singularities [4,5] are important both for experiments [6] and numerical calculations [7–9]. For a more comprehensive discussion of Griffiths-McCoy singularities in a myriad of disordered models and on the role of disorder in general in quantum critical behavior; see Ref. [10].

In this work, we study the critical behavior and Griffiths-McCoy singularities in the dilute transverse-field Ising model [9,11] at $T = 0$ using numerical linked cluster expansions (NLCEs) [12–15]. We use NLCEs to study the susceptibility, magnetization, and structure factor and establish the phase diagram of the system. We pay special attention to the existence of Griffiths-McCoy singularities, finding numerical evidence for their existence in the behavior of the magnetization as a function of longitudinal field and the probability distribution of the local susceptibility.

II. OVERVIEW OF APPROACH

A. Model

We consider the zero-temperature behavior of a site-diluted transverse-field Ising model on a two-dimensional square lattice. The model is parametrized by three values $\{J, h, p\}$, where J is an exchange constant that controls the strength of nearest-neighbor spin-spin interactions, h is the coupling strength to a transverse field, and p is the dilution parameter.

The Hamiltonian of the model is

$$\mathscr{H} = J \sum_{\langle i,j \rangle} \epsilon_i \epsilon_j \sigma_i^z \sigma_j^z + h \sum_i \epsilon_i \sigma_i^x, \tag{1}$$

where $\langle \cdot, \cdot \rangle$ denotes nearest-neighbor pairs of sites on the lattice and σ^z and σ^x are the Pauli matrices. The ϵ_i terms are site dilution variables: quenched random variables with bimodal distribution, taking values of 0 and 1 with probability p and $1 - p$, respectively.

At zero temperature, thermal averages reduce to ground-state expectation values. We denote the ground state by $|0\rangle$. We will take $J < 0$ to study the ferromagnetic problem. The ground state only depends on the ratio h/J. Hence, we set $J = -1$.

B. Method

Numerical linked cluster expansions (NLCEs) is a method of approximating an extensive property of a thermodynamic system as a series with terms computed by exact diagonalization of small, finite-size systems—"clusters"—which embed into the lattice of the full model. Specifically, given an extensive property P, its per-site value in the thermodynamic limit is given by the expression

$$\lim_{N\to\infty} \frac{P}{N} = \sum_c L[c] W[c]. \tag{2}$$

The lattice constant $L[c]$ denotes the number of ways, per site, the cluster c can embed into the lattice. $W[c]$ is the weight of the cluster in the lattice, determined recursively by

$$W[c] = P[c] - \sum_{c' \subset c} W[c'], \tag{3}$$

where $c' \subset c$ is a subcluster—a cluster which embeds into cluster c—and $P[c]$ is the property computed on the cluster.

For disordered models, one is typically interested in quantities of the form $[P/N]_{\text{av}}$, where $[\ldots]_{\text{av}}$ denotes the quenched average. In our case, this is a sum over the site dilution variables ϵ_i. NLCE can be generalized to a quenched average in a straightforward way by simply computing the quenched average of each cluster individually before summing up the total value of the property [16–18]. In the case of the site-diluted model we study, this greatly simplifies the resulting series. For any cluster, any configuration of the site dilution variables ϵ_i in which any site is omitted, will reduce the cluster to a collection of its subclusters, resulting in zero weight after the weights of subclusters are subtracted away. Only the single configuration with no dilution survives the subgraph subtraction. Consequently, the NLCE of the quenched average of a property P reduces to simply the NLCE of P for the pure system with an additional factor of $p^{N[c]}$, the probability of the nondilute configuration:

$$\lim_{N\to\infty} \left[\frac{P}{N}\right]_{\text{av}} = \sum_c L[c] W[c] p^{N[c]} \equiv \sum_{n=1}^{\infty} a_n p^n, \tag{4}$$

where $N[c]$ denotes the number of sites in c. As a consequence, the NLCE becomes a power series in the dilution parameter p.

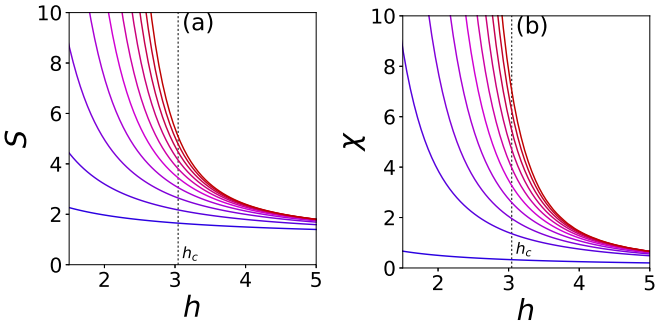

FIG. 1. Panel (a) shows the structure factor S and panel (b) shows the susceptibility χ. For both quantities, the NLCE produces a series expansion in the number of bonds in clusters. Our analysis includes clusters up to order 10. Curves of order 1–10 in the number of bonds are shown simultaneously with increasing redness starting with blue at first order. The NLCE converge well for $h > h_c$ and increase sharply close to h_c before saturating for small values of h. The point at which the steep rise begins occurs closer and closer to h_c the higher the order.

III. PURE SYSTEM ANALYSIS

We first considered the nondilute Ising problem (the $p = 1$ limit). We calculate the susceptibility and structure factor, as both of these quantities are known to diverge strongly near the pure system's critical point of $h_c \simeq 3.044$. The structure factor S is defined by

$$S = \sum_{i,j} \langle \sigma_i^z \sigma_j^z \rangle - \langle \sigma_i^z \rangle \langle \sigma_j^z \rangle, \tag{5}$$

where we use the notation $\langle \sigma_i^z \rangle = \langle 0 | \sigma_i^z | 0 \rangle$. To compute the susceptibility, we add an additional longitudinal-field term to the Hamiltonian:

$$\mathscr{H} = J \sum_{\langle i,j \rangle} \sigma_i^z \sigma_j^z + h \sum_i \sigma_i^x + h_L \sum_i \sigma_i^z. \tag{6}$$

With this additional factor, letting E_0 denote the ground-state energy, the susceptibility is given by

$$\chi = -\lim_{h_L \to 0} \frac{\partial^2 E_0}{\partial {h_L}^2}. \tag{7}$$

The ground state of a finite-size system is straightforward to compute numerically. Consequently, we are able to use NLCE [12–15] to compute the ground-state energy E_0 and structure factor S. By computing E_0 for a range of h_L, numerically finding the second derivative via the central difference method, and evaluating the result for small h_L, we obtain a reasonable estimate for the susceptibility χ. The results of the computation are shown in Fig. 1. Without help of an extrapolation method it is difficult to locate the critical point in NLCE because the structure factor and susceptibility keep on increasing as h is reduced in each order. However, we can do better by including an additional "mean-field" term in the Hamiltonian at the boundary of each cluster to account for the effects of the rest of the lattice:

$$\mathscr{H} = J \sum_{\langle i,j \rangle} \sigma_i^z \sigma_j^z + h \sum_i \sigma_i^x + m(h) \sum_i q_i[c] \sigma_i^z. \tag{8}$$

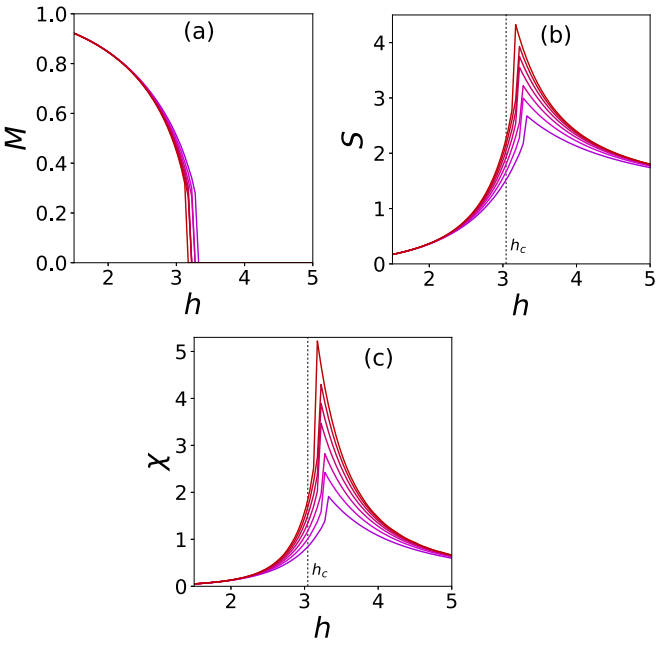

FIG. 2. In all three plots, orders 4–10 in the number of bonds are shown, with higher orders shown in redder colors. Panel (a) shows the magnetization computed by using the self-consistency constraint. Its shape is qualitatively typical for the magnetization of a ferromagnet, falling to zero near the critical point. Panels (b) and (c) show curves of the structure factor S and susceptibility χ plotted by using the magnetization self-consistent mean field. Both quantities now converge very well in both the ordered and disordered phases, peaking near the critical point.

This added term is a mean field acting on the boundary of the cluster: the quantity $q_i[c]$ represents the number of neighbors on the site i that are not in the cluster c and so are outside the cluster. We expect the h-dependent value of m to satisfy the self-consistency condition $m = M$, where M is the magnetization per site of the lattice, defined by

$$M = \frac{1}{N}\sum_i \langle \sigma_i^z \rangle. \tag{9}$$

We implement this as a constraint numerically by computing M for a small number of guessed, constant values of m for each h, then interpolating to find the approximate value of m satisfying the self-consistency constraint. Computed for a range of h, this gives an approximation for the magnetization M and also regulates the convergence of the NLCE for both S and χ. The result of this computation is shown in Fig. 2. This gives a qualitative picture of the phase transition but is not accurate enough to calculate critical properties. In this paper, we are not interested in a more complex extrapolation of the NLCE series, because our primary interest is in the diluted system which turns out to be much more straightforward to extrapolate.

IV. DILUTION PROBLEM

A. Phase diagram

We now turn our attention to the dilute Ising problem. In the limit of $h \to 0$, this becomes a percolation problem with two phases controlled by the value of the percolation parameter p. At low values of p, highly dilute configurations dominate, the lattice becomes a collection of disconnected clusters, and no long-range order develops. Above the percolation threshold $p_c \simeq 0.59$, the lattice percolates, with an infinite cluster spanning the full length of the lattice. This infinite cluster of spins can develop long-range order. For small, nonzero values of h, it has been shown [1,2] that a flat phase boundary with p_c independent of h extends into the h-p plane to some value h_M with a lower bound of $h = 1$, the critical point of the one-dimensional model. Near the critical point h_c of the pure system, the phase boundary is believed to extend smoothly downward into the plane before meeting the flat boundary at the multicritical point h_M. We used NLCE to confirm this picture of the phase diagram and get an estimate of h_M, the results of which can be visualized in Fig. 3(a).

Due to the simplification of NLCE to a power series as given by Eq. (4), we are able to use the ratio method [19] to extrapolate how the critical point p_c varies as a function of h. Specifically, for values of p near p_c, we expect the structure factor S to obey an asymptotic power law: $S \propto (p - p_c)^{-\gamma}$. Consequently, we expect the coefficients of the power series for S from Eq. (4) to obey (up to corrections of order $1/n^2$):

$$\frac{a_n}{a_{n-1}} = \frac{1}{p_c}\left(1 + \frac{\gamma - 1}{n}\right). \tag{10}$$

This can be seen by matching powers of p in the series expansions resulting from taking the derivative of Eq. (4) and the power law for S. A plot of these ratios is shown in Fig. 4 for a range of values of h.

One can estimate p_c at a given h from the intercept of a regression of these ratios computed for that h. We use this method to compute p_c as a function of h. The resulting phase diagram is shown in Fig. 3(a).

In addition to this, the slope of the linear regression ratios can be used to approximate the critical exponent γ. Note that this is not the standard γ exponent because we are not calculating the susceptibility. The susceptibility itself develops strong Griffiths-McCoy singularities and hence cannot be used to study the critical point by a series expansion method [20]. In the region where this method converges well and is physically meaningful, γ is approximately constant in the range (0.5 to 0.6), within our limited accuracy, as shown in Fig. 3(b). The susceptibility at this transition is known to have an activated dynamical scaling behavior with a divergent dynamical critical exponent z [11,21–23]; however, the equal-time structure factor can still have a power-law behavior. The strong-disorder fixed-point studies by real-space renormalization group [22] and Monte Carlo simulations [21,23] do give a power-law singularity for the structure factor, but with a very small exponent $\gamma < 0.1$. Our results are clearly not in agreement with them. This may mean that the series obtained is too short to access the strong-disorder fixed point and instead gives a conventional random fixed point relevant at intermediate length scales. We then compare our results with the double epsilon expansion of Boyanovsky and Cardy [24]. They considered the problem of impurities correlated along some directions. Our quantum problem corresponds to the case of two physical dimensions plus one correlated dimension for a total of three dimensions. Setting $\epsilon_d = 1$

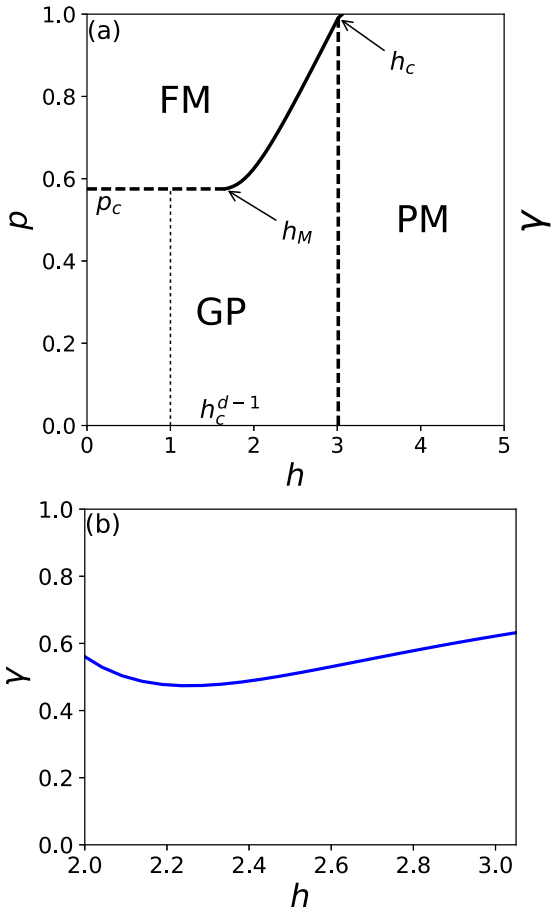

FIG. 3. (a) Phase diagram, showing distinct ferromagnetic (FM), paramagnetic (PM), and Griffiths (GP) phases. Using linear regression on data like that shown in Fig. 4 for many values of h, we established the boundary shown by the full line. This line begins at the approximate h_c of the pure system, which we find to be 3.03, close to the known value of 3.04. The flat continuation of the phase boundary we expect after convergence of the NLCE breaks down for $h < h_M$ is shown by the horizontal dashed line. This point begins at $h_M \simeq 1.65$. This line intersects the p axis at the percolation probability p_c, which we find to be 0.58, also close to the known value of 0.59. The dotted line marked with h_c^{d-1} shows the value of the one-dimensional critical point, a lower bound on h_M. The vertical dashed line indicates a separation between the ordinary paramagnetic phase and the disordered Griffiths phase where we observe Griffiths-McCoy singularities to be present. Panel (b) shows the value of γ computed from the slope of the same linear regression. This gives the rough bounds $0.47 \lesssim \gamma \lesssim 0.61$.

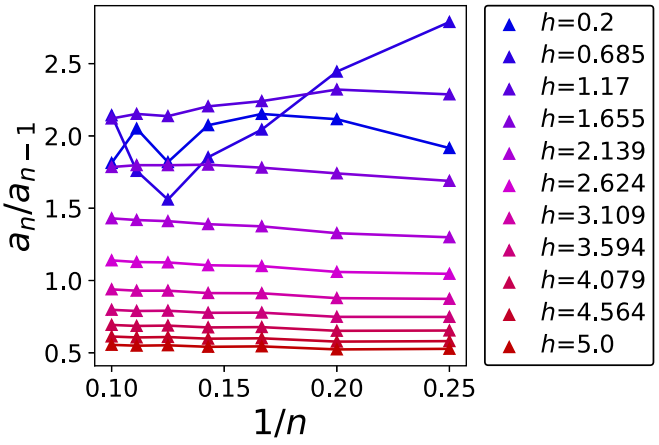

FIG. 4. Plots of ratios a_n/a_{n-1} as a function of $1/n$ for a representative range of h values with n ranging from 4 to 10. For large values of h, these plots are all relatively flat. For values of $h \lesssim h_c$, the intercept of a linear regression of the values shown here will yield a value of $1/p_c$ that is <1. This implies an absence of any phase transition in the physically relevant range of p values in the system. Subsequently, the h at which the computed p_c becomes unity gives an approximation of the pure system critical point h_c. Additionally, for sufficiently small values of h, the plots become very nonlinear and irregular, indicating that the convergence of NLCE breaks down below some h_M. This is to be expected as at the multicritical point h_M critical behavior switches from being governed by the value of h to being controlled by the geometry of the lattice, and the singularity is no longer a power-law for h below h_M.

and $\epsilon = 4 - d = 1$ into the expressions of Boyanovsky and Cardy [24], one obtains the divergence of the structure factor exponent to be $\gamma = (2 - \eta - z)\nu \approx 0.73$. Given the level of accuracy of our calculations and that this is leading order in the epsilon expansions, the agreement is not unreasonable. As the phase diagram flattens out the series loses convergence. This is because the system no longer has a power-law singularity. We estimate that the phase diagram is flat below $h_M \approx 1.65$. Again, we are not aware of previous accurate estimates of h_M, which is not easy to obtain in quantum Monte Carlo simulations [9].

B. Griffiths-McCoy singularities

Griffiths-McCoy (GM) singularities occur in disordered quantum models where the pure system would be ordered. Rare, ordered regions can locally mimic the ordered phase of the pure system. Here we focus on the low p and h regime—the Griffiths phase on the disordered side—as nondilute regions in an otherwise highly dilute lattice. This region is shown in Fig. 3(a) labeled GP. There are Griffiths singularities also on the ordered side, but we will not study them here as in the absence of a mean-field the NLCE will not converge there.

We expect GM singularities to manifest in the behavior of the time-integrated or zero-frequency response of the system as well as in the magnetization M as a function of the longitudinal external field h_L:

$$\mathscr{H} = J \sum_{\langle i,j \rangle} \epsilon_i \epsilon_j \sigma_i^z \sigma_j^z + h \sum_i \epsilon_i \sigma_i^x + h_L \sum_i \epsilon_i \sigma_i^z. \qquad (11)$$

The magnetization as a function of longitudinal field of a pure ferromagnet in its paramagnetic phase is linear in the limit of small h_L. However, below the percolation threshold in the diluted model, we expect the presence of GM singularities to alter this power law behavior and produce a nonlinear relationship between M and h_L. In agreement with this picture, we find that the magnetization vs h_L curve develops curvature for values of h below h_c as shown in Fig. 5. Specifically, the magnetization obeys some nonlinear power law $M \sim {h_L}^a$. To quantify how the exponent varies with h, we use a linear fit of a log-log plot of M and h_L to compute a for a range of values

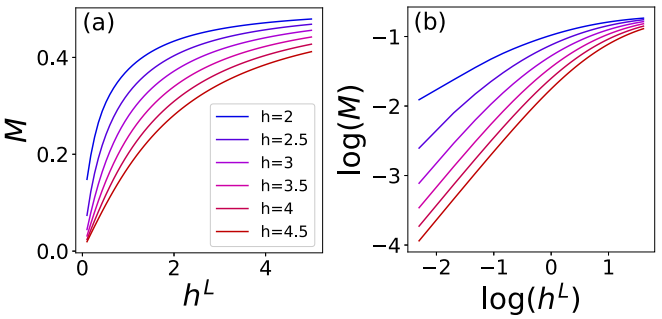

FIG. 5. Both plots show computations for $p = 0.5$, well below the percolation threshold $p_c = 0.59$ and in the Griffiths phase for small h. Computations were done to 10th order in the number of sites. Panel (a) shows magnetization M plotted as a function of longitudinal field h_L for a representative range of h values. Below the critical point $h_c = 3.04$, curvature begins to develop in the small-h_L limit. This can be better visualized in panel (b), showing a log-log plot of the same quantities. For $h > h_c$, the slopes of the log-log plot are about 1, while for values $h < h_c$, they are noticeably less than 1.

of h. As shown in Fig. 6, for $h < h_c$, this varies continuously as a function of h.

As an additional indication of the influence of GM singularities, we consider the probability distribution of the local susceptibility $\chi_{\rm loc} = \sum_i \chi_i$, with the one-site susceptibility defined by adding a one-site longitudinal term to the Hamiltonian:

$$\mathscr{H} = J \sum_{\langle i,j \rangle} \epsilon_i \epsilon_j \sigma_i^z \sigma_j^z + h \sum_i \epsilon_i \sigma_i^x + h_L \epsilon_i \sigma_i^z. \qquad (12)$$

The one-site susceptibility is then given by

$$\chi_i = -\lim_{h_L \to 0} \frac{\partial^2 E_0}{\partial {h_L}^2}. \qquad (13)$$

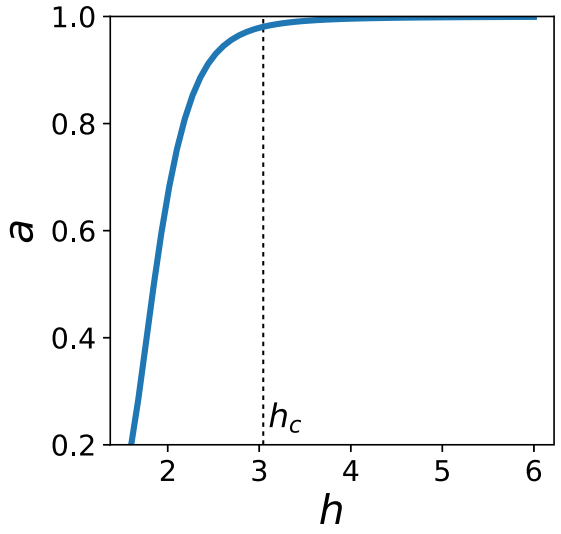

FIG. 6. Plot of the exponent a as a function of h for $p = 0.5$. For $h > h_c$, $a \simeq 1$ as is typical of the pure system. For $h < h_c$, a begins decreasing continuously with h, indicating the influence of GM singularities.

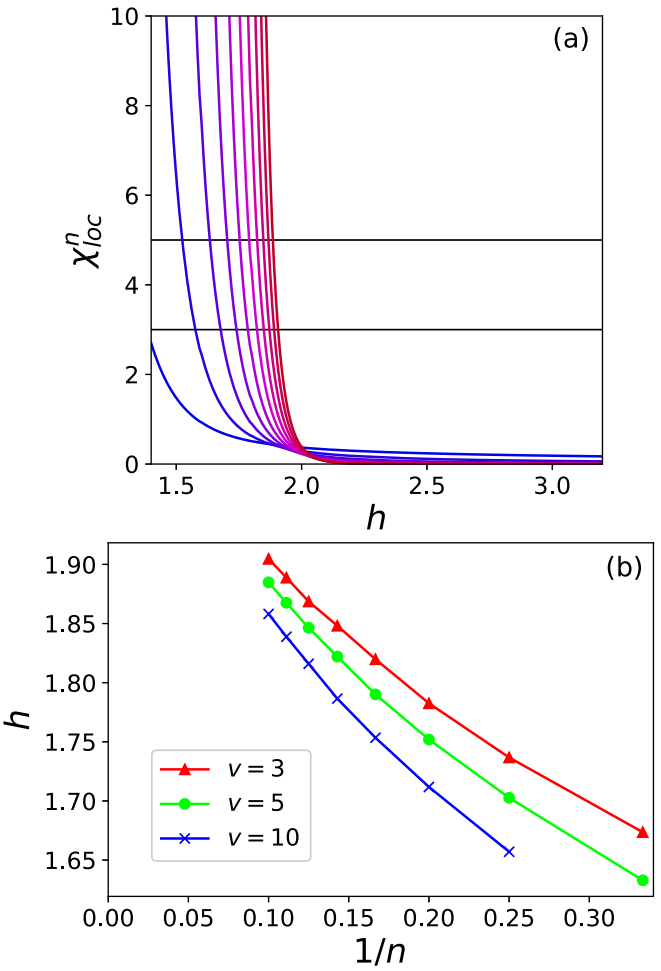

FIG. 7. Panel (a) shows plots of the moments of the local susceptibility $\chi^n_{\rm loc}$ shown for $p = 0.5$ for n ranging from 1 to 10, with smaller n values appearing in blue and larger n values in red. All values were computed to 10th order in the number of sites. Panel (b) shows a series of points where each moment crosses a selection of values v [indicated by horizontal lines in panel (a)], indicating roughly where each moment begins to diverge, plotted as a function of $1/n$. As n is increased, these plots begin to curve up pushing them towards h_c.

We study this distribution by examining its moments $\chi^n_{\rm loc} \equiv \sum_i \chi_i^n$. For small values of n, the value of h at which the moments begin to diverge is typically much smaller than the pure system critical point h_c, but as n is increased, the point moves closer to h_c. Curves for the moments plotted over a range of values of h and their points of divergence as a function of $1/n$ are shown in Figs. 7(a) and 7(b), respectively. This movement of the divergence point is indicative of tails in the probability distribution of $\chi_{\rm loc}$ induced by the presence of GM singularities. Theoretically, the singularities set in as soon as one goes past h_c of the pure system. However, near h_c they are weak and consequently only some high moments may diverge. As one goes deeper into the Griffiths phase, the singularities become stronger and, as a result, lower moments diverge as well.

V. CONCLUSION

In this work, we have used NLCE to compute the magnetization, structure factor, and susceptibility of the zero-temperature dilute quantum transverse-field Ising model. In analyzing the pure system, we demonstrated the efficacy of the NLCE at computing the magnetization as a function of transverse field strength h by adding to the Hamiltonian a mean-field term coupled to the boundary of each cluster and imposing a self-consistency constraint on the strength of the coupling and the magnetization. This regulates the convergence of the NLCE in the ordered phase for the structure factor and susceptibility. It yields an approximation that converges reasonably in both the low- and high-h regimes. Although, in the absence of more sophisticated sequence extrapolations, it is not accurate enough to study critical phenomena.

In the problem with dilution, NLCE turns into a series expansion in the dilution parameter. Hence, we used a series extrapolation method to study the asymptotic behavior of the structure factor to compute p_c as a function of h, leading to the phase boundary. This also gave us a good estimate of the pure system critical point at $h_c \simeq 3.03$ and the percolation threshold $p_c \simeq 0.58$, in reasonable agreement with known results of 3.04 and 0.59, respectively. Additionally, we found the multicritical point at which the phase boundary flattens to be at $h_M \simeq 1.65$, above the known lower bound of 1. For the random system we found the structure factor to diverge with an exponent γ of $0.47 \lesssim \gamma \lesssim 0.61$, whose accuracy is difficult to gauge. It is quite far from the value of less than 0.1 found at the strong-disorder fixed point [21–23] but is not far from a more conventional random fixed point studied by Boyanovsky and Cardy who obtained [24] a γ value of 0.73.

For small values of p and h, we found numerical evidence for Griffiths-McCoy singularities in the behavior of the magnetization as a function of longitudinal field and moments of the local susceptibility. In low-p regions of the paramagnetic phase, the slope a of the magnetization as a function of small h_L remains roughly constant at 1 for all values of h. However, at values below h_c we found that a continuously diminished as a function of h, implying that the magnetization becomes nonlinear. This behavior mirrors observation from experiments, such as in Ref. [6]. Additionally, in this region, the moments of the local susceptibility diverge at points $h < h_c$, with higher moments diverging for values of h closer to h_c, indicating the presence of tails in the probability distribution of the local susceptibility. Both of these effects evince a change in behavior when crossing below h_c in the low-p regime, demonstrating the existence of the Griffiths phase dominated by Griffiths-McCoy singularities.

The NLCE method has been applied successfully to Heisenberg spin models as well as to $t-J$ and other fermion models [12–14], including diluted systems at high temperatures. It can also be used to study GM singularities, when these systems are diluted at $T = 0$ or at low temperatures. This is left for future study.

ACKNOWLEDGMENTS

This work was supported by the National Science Foundation DMR Grant No. 1855111 and through an REU program by the US National Science Foundation (Grant No. PHY-1560482).

[1] A. B. Harris, J. Phys. C: Solid State Phys. **7**, 3082 (1974).
[2] R. B. Stinchcombe, J. Phys. C: Solid State Phys. **14**, L263 (1981).
[3] R. B. Griffiths, Phys. Rev. Lett. **23**, 17 (1969).
[4] B. M. McCoy, Phys. Rev. Lett. **23**, 383 (1969).
[5] B. M. McCoy, Phys. Rev. **188**, 1014 (1969).
[6] R. Wang, A. Gebretsadik, S. Ubaid-Kassis, A. Schroeder, T. Vojta, P. Baker, F. L. Pratt, S. J. Blundell, T. Lancaster, I. Franke *et al.*, Phys. Rev. Lett. **118**, 267202 (2017).
[7] H. Rieger and A. P. Young, Phys. Rev. Lett. **72**, 4141 (1994).
[8] M. Guo, R. N. Bhatt, and D. A. Huse, Phys. Rev. Lett. **72**, 4137 (1994).
[9] T. Ikegami, S. Miyashita, and H. Reiger, J. Phys. Soc. Jpn. **67**, 2671 (1998).
[10] T. Vojta, J. Low Temp. Phys. **161**, 299 (2010).
[11] T. Senthil and S. Sachdev, Phys. Rev. Lett. **77**, 5292 (1996).
[12] M. Rigol, T. Bryant, and R. R. P. Singh, Phys. Rev. Lett. **97**, 187202 (2006).
[13] M. Rigol, T. Bryant, and R. R. P. Singh, Phys. Rev. E **75**, 061118 (2007).
[14] B. Tang, E. Khatami, and M. Rigol, Comput. Phys. Commun. **184**, 557 (2013).
[15] A. B. Kallin, K. Hyatt, R. R. P. Singh, and R. G. Melko, Phys. Rev. Lett. **110**, 135702 (2013).
[16] B. Tang, D. Iyer, and M. Rigol, Phys. Rev. B **91**, 161109 (2015).
[17] T. Devakul and R. R. P. Singh, Phys. Rev. Lett. **115**, 187201 (2015).
[18] M. Mulanix, D. Almada, and E. Khatami, arXiv:1810.12901.
[19] J. Oitmaa, C. Hamer, and W. Zheng, *Series Expansion Methods for Strongly Interacting Lattice Models* (Cambridge University Press, Cambridge, 2006).
[20] R. R. P. Singh and A. P. Young, Phys. Rev. E **96**, 022139 (2017).
[21] Y.-C. Lin, N. Kawashima, F. Iglói, and H. Rieger, Prog. Theor. Phys. Suppl. **138**, 479 (2000).
[22] I. A. Kovács and F. Iglói, Phys. Rev. B **82**, 054437 (2010).
[23] C. Pich, A. P. Young, H. Rieger, and N. Kawashima, Phys. Rev. Lett. **81**, 5916 (1998).
[24] D. Boyanovsky and J. L. Cardy, Phys. Rev. B **26**, 154 (1982).